PHYSICAL REVIEW B **82**, 014428 (2010)

Spin-orbit coupling and spin waves in ultrathin ferromagnets: The spin-wave Rashba effect

A. T. Costa,[1] R. B. Muniz,[1] S. Lounis,[2] A. B. Klautau,[3] and D. L. Mills[2]
[1]*Instituto de Física, Universidade Federal Fluminense, 24210-340 Niterói, RJ, Brazil*
[2]*Department of Physics and Astronomy, University of California, Irvine, California 92697, USA*
[3]*Departamento de Fisica, Universidade Federal do Pará, Belém, PA, Brazil*

(Received 18 April 2010; revised manuscript received 3 June 2010; published 29 July 2010)

We present theoretical studies of the influence of spin-orbit coupling on the spin-wave excitations of the Fe monolayer and bilayer on the W(110) surface. The Dzyaloshinskii-Moriya interaction is active in such films by virtue of the absence of reflection symmetry in the plane of the film. When the magnetization is in plane, this leads to a linear term in the spin-wave dispersion relation for propagation perpendicular to the magnetization, to produce a dispersion curve similar in nature to that found for electrons on semiconducting surfaces when the Rashba coupling is active. We also show spin-polarized electron-loss spectroscopy response functions that illustrate the role of spin-orbit coupling in such measurements. In addition to the modifications of the dispersion relations for spin waves, the presence of spin-orbit coupling in the W substrate leads to a substantial increase in the linewidth of the spin-wave modes. The formalism we have developed applies to a wide range of systems, and the particular system explored in the numerical calculations provides us with an illustration of phenomena which will be present in other ultrathin ferromagnet/substrate combinations.

DOI: 10.1103/PhysRevB.82.014428 PACS number(s): 75.30.Ds, 75.30.Gw

I. INTRODUCTION

The study of spin dynamics in ultrathin ferromagnets is of fundamental interest, since new physics arises in these materials that has no counterpart in bulk magnetism. Examples are provided by relaxation mechanisms evident in ferromagnetic resonance (FMR) and Brillouin light-scattering studies,[1–3] and also for the large wave vectors probed by spin-polarized electron-loss spectroscopy (SPEELS).[4] Of course, by now the remarkable impact of ultrathin film structures on magnetic data storage is very well known and other applications that exploit spin dynamics in such materials are envisioned. Thus these issues are important from a practical point of view as well as from that of fundamental physics.

Theoretical studies of the nature of spin waves in ultrathin films adsorbed on metal substrates have been carried out for some years now, along with comparison with descriptions provided with the Heisenberg model.[5,6] In this paper, we extend the earlier theoretical treatments to include the influence of spin-orbit coupling on the spin-wave spectrum of ultrathin films. This extension is motivated by a most interesting discussion of the ground state of the Mn monolayer on the W(110) surface. A nonrelativistic theoretical study of this system predicted that the ground state would be antiferromagnetic in character.[7] This prediction was confirmed by spin-polarized scanning tunneling microscope studies of the system.[8] However, recent experimental STM data with a more sensitive instrument showed a more complex ground state, wherein the ground state is, in fact, a spin-density wave.[9] One can construct the new state by beginning with the antiferromagnet and then superimposing on this a long-wavelength modulation on the direction of the moments on the lattice. The authors of Ref. 9 argued that the lack of reflection symmetry of the system in the plane of the film activates the Dzyaloshinskii-Moriya (DM) interaction, and the new state has its origin in this interaction. They also presented relativistic *ab initio* calculations that gave an excellent account of the new data. The reflection symmetry is broken simply by the presence of the substrate upon which the film is grown. This argument to us is most intriguing, since one can then conclude that the DM interaction must be active in any ultrathin ferromagnet; the substrate is surely always present. The DM interaction has its origin in the spin-orbit interaction, which of course is generally very weak in magnets that incorporate the 3*d* transition elements as the moment bearing entities. However, in the case of the Mn monolayer on W(110) hybridization between the Mn 3*d* and the W 5*d* orbitals activates the very large W spin-orbit coupling with the consequence that the strength of the DM interaction can be substantial, as illustrated by the calculations presented in Ref. 9. One may expect to see substantial impact of the DM interaction in other ultrathin magnets grown on 5*d* substrates and possibly 4*d* substrates as well.

Another magnetic film/substrate combination that has been extensively studied is Fe on W(110). Recent calculations based on the adiabatic approximation[10] predicted the existence of left/right asymmetry in the spin-wave energies. Also recent experimental results[11] have shown asymmetry from the same origin in the line shape of spin excitations measured by SPEELS.

We have here another example of new physics present in ultrathin magnets that is not encountered in the bulk form of the material from which the ultrathin structure is fabricated. The purpose of this paper is to present our theoretical studies of spin-orbit effects on spin waves and also on the dynamic susceptibility of a much studied ultrathin film/substrate combination, the Fe monolayer and bilayer on W(110). We find striking effects. For instance, when the magnetization is in plane, as we shall see the DM interaction introduces a term linear in wave vector in the dispersion relation of spin waves. This leads to a dispersion curve very similar in nature to that found for electrons on semiconducting surfaces where Rashba coupling is active. In the ferromagnet, however, time-reversal symmetry is broken and there is only one branch to the dispersion curve; the presence of time-reversal symmetry requires two branches, one the mirror image of the other, for electrons on semiconductor surfaces. A consequence of the linear term is that the uniform spin-wave mode at zero wave vector acquires a finite group velocity. We find this to be in the range of 2×10^5 cm/s for the Fe monolayer on W(110). Furthermore, left/right asymmetries appear in the SPEELS response functions. Thus, we shall see that spin-orbit coupling has clear effects on the spin excitations of transition-metal ultrathin ferromagnets grown on $5d$ substrates.

We comment briefly on the philosophy of the approach used here and in various earlier publications.[5] Numerous authors proceed as follows. One may generate a description of the magnetic ground state of the adsorbed films by means of an electronic-structure calculation based on density-functional theory (DFT). It is then possible to calculate, within the framework of an adiabatic approximation, effective Heisenberg exchange integrals J_{ij} between the magnetic moments in unit cell i and unit cell j. These may be entered into a Heisenberg Hamiltonian, and then spin-wave dispersion relations may be calculated through use of spin-wave theory. It has been known for decades[12] that in the itinerant $3d$ magnets, effective exchange interactions calculated in such a manner have very long range in real space. Thus, one must include a very large number of distant neighbors in order to obtain converged results. This is very demanding to do with high accuracy for the very numerous distant neighbors, since the exchange interactions become very small as one moves out into distant neighbor shells.

At a more fundamental level, as noted briefly above, discussions in earlier publications show that in systems such as we study here, the adiabatic approximation breaks down badly with qualitative consequences.[5] First, spin-wave modes of finite wave vector have very short lifetimes, by virtue of decay into the continuum of particle-hole pairs (Stoner excitations) even at the absolute zero of temperature[5,13] whereas in Heisenberg model descriptions their lifetime is infinite. In multilayer films, the earlier calculations show that as a consequence of the short lifetime, the spectrum of spin fluctuations at large wave vectors contains a single broad feature which disperses with wave vector in a manner similar to that of a spin wave; this is consistent with SPEELS data on an eight-layer film of Co on Cu(100).[4] This picture stands in contrast to that offered by the Heisenberg model, in which a film of N layers has N spin-wave modes for each wave vector and each mode has infinite lifetime.

The method developed earlier, and extended here to incorporate spin-orbit coupling, takes due account of the breakdown of the adiabatic approximation and also circumvents the need to calculate effective exchange interactions in real space out to distant neighbor shells. We work directly in wave-vector space through study of the wave-vector- and frequency-dependent susceptibilities discussed below, denoted as $\chi_{+,-}(\vec{Q}_{\parallel},\Omega;l_{\perp},l'_{\perp})$. The imaginary part of this object, evaluated for $l_{\perp}=l'_{\perp}$ and considered as a function of frequency Ω for fixed wave vector $\vec{Q}_{\parallel}$ provides us with the frequency spectrum of spin fluctuations on layer $l_{\perp}$ for the wave vector chosen. Spin waves appear as peaks in this function, very much as they do in SPEELS data, and in a manner very similar to that used by experimentalist we extract a dispersion relation for spin waves by following the wave-vector dependence of the peak frequency. We never need to resort to a real-space summation procedure over large number of neighbors, coupled by very tiny exchange couplings. The spin-wave exchange stiffness can be extracted either by fitting the small wave-vector limit of the dispersion relation so determined or alternatively by utilizing an expression derived earlier[5] which once again does not require a summation in real space.

We comment on another feature of the present study. In earlier calculations,[5,13,14] as in the present paper, an empirical tight-binding description forms the basis for our description of the electronic structure. Within this approach, referred to as a multiband Hubbard model, we can generate the wave-vector- and frequency-dependent susceptibilities for large systems. In the earlier papers, effective tight-binding parameters were extracted from bulk electronic-structure calculations. The present studies are based on tight-binding parameters obtained directly from a real-space linear muffin-tin orbital atomic sphere approximation (RS-LMTO-ASA) calculation for the Fe/W(110) system. We also obtain tight-binding parameters by fitting Korringa Kohn Rostoker (KKR)-based electronic-structure calculations for the ultrathin film/substrate combinations of interest. We find that spin waves in the Fe/W(110) system are quite sensitive to the empirical tight-binding parameters which are employed, though as we shall see the various descriptions provide very similar pictures of the one-electron local density of states.

We note that Udvardi and Szunyogh[10] have also discussed the influence of spin-orbit coupling on the dispersion relation of spin waves in the Fe monolayer on W(110) within the framework of the adiabatic approach discussed above, where exchange interactions and other magnetic parameters are calculated in real space. We shall discuss a comparison with our results and theirs below. There are differences. Additionally and very recently, Bergman *et al.*[15] investigated within an adiabatic approach finite-temperature effects on the magnon spectrum of Fe/W(110).

In Sec. II, we comment on our means of introducing spin-orbit coupling into the theory. The results of our calculations are summarized in Sec. III and concluding remarks are found in Sec. IV.

II. CALCULATION OF THE DYNAMIC SUSCEPTIBILITY IN THE PRESENCE OF SPIN-ORBIT COUPLING

The formalism for including spin-orbit coupling effects in our description of spin dynamics is quite involved, so in this section we confine our attention to an outline of the key steps, and an exposition of the overall structure of the theory. Our starting point is the multiband Hubbard model of the system that was employed in our earlier study of spin dynamics in ultrathin ferromagnets. The starting Hamiltonian is written as[5]

$$H=\sum_{ij}\sum_{\mu\nu\sigma}T_{ij}^{\mu\nu}c_{i\mu\sigma}^{\dagger}c_{j\nu\sigma}+\frac{1}{2}\sum_{\mu\nu\mu'\nu'}\sum_{i\sigma\sigma'}U_{i;\mu\nu,\mu'\nu'}c_{i\mu\sigma}^{\dagger}c_{i\nu\sigma'}^{\dagger}c_{i\nu'\sigma'}c_{i\mu'\sigma},\qquad(1)$$

where i and j are site indices, σ,σ' refer to spin, and μ,ν to the tight-binding orbitals, nine in number for each site, which are included in our treatment. The Coulomb interactions operate only within the $3d$ orbitals on a given lattice site. The film, within which ferromagnetism is driven by the Coulomb interactions, sits on a semi-infinite substrate within which the Coulomb interaction is ignored.

In our empirical tight-binding picture, the spin-orbit interaction adds a term we write as

$$H_{SO}=\sum_{i}\sum_{\mu\nu}\frac{\lambda_i}{2}[L_{\mu\nu}^{z}(c_{i\mu\uparrow}^{\dagger}c_{i\nu\uparrow}-c_{i\mu\downarrow}^{\dagger}c_{i\nu\downarrow})+L_{\mu\nu}^{+}c_{i\mu\downarrow}^{\dagger}c_{i\nu\uparrow}+L_{\mu\nu}^{-}c_{i\mu\uparrow}^{\dagger}c_{i\nu\downarrow}],\qquad(2)$$

where $\vec{L}$ is the angular momentum operator, λ_i is the local spin-orbit coupling constant, $L^{\pm}=L^{x}\pm iL^{y}$ and $L_{\mu\nu}^{\alpha}=\langle\mu|L^{\alpha}|\nu\rangle$. We assume that the spin-orbit interaction, present both within the ferromagnetic film and the substrate, operates only within the $3d$ atomic orbitals. A convenient tabulation of matrix elements of the orbital angular-momentum operators is found in Ref. 16.

Information on the spin waves follows from the study of the spectral density of the transverse dynamic susceptibility $\chi_{+,-}(\vec{Q}_{\parallel},\Omega;l_{\perp},l'_{\perp})$ as discussed above. From the text around Eq. (1) of Ref. 14, we see that this function describes the amplitude of the transverse spin motion (the expectation value of the spin operator S^{+} in the layer labeled $l_{\perp}$) in response to a fictitious transverse magnetic field of frequency Ω and wave vector $\vec{Q}_{\parallel}$ parallel to the film surface that is applied to layer $l'_{\perp}$ of the sample. The spectral density, given by $\mathrm{Im}\{\chi_{+,-}(\vec{Q}_{\parallel},\Omega;l_{\perp},l'_{\perp})\}$, when multiplied by the Bose-Einstein function $n(\Omega)=[\exp(\beta\Omega)-1]^{-1}$ is also the amplitude of thermal spin fluctuations of wave vector $\vec{Q}_{\parallel}$ and frequency Ω in layer $l_{\perp}$. We obtain information regarding the character (frequency, linewidth, and amplitude in layer $l_{\perp}$) of spin waves from the study of this function, as discussed earlier.[5]

Our previous analyses are based on the study of the dynamic susceptibility just described through use of the random-phase approximation (RPA) of many-body theory. The Feynman diagrams included in this method are the same as those incorporated into time-dependent density-functional theory, though use of our Hubbard model allows us to solve the resulting equation easily once the very large array of irreducible particle-hole propagators are generated numerically.

Our task in the present paper is to extend the RPA treatment to incorporate spin-orbit coupling. The extension is nontrivial. The quantity of interest, referred to in abbreviated notation as $\chi_{+,-}$, may be expressed as a commutator of the spin operators S^{+} and S^{-} whose precise definition is given earlier.[5,10] With spin-orbit coupling ignored, the RPA decoupling procedure leads to a closed equation for $\chi_{+,-}$. When the RPA decoupling is carried out in its presence, we are led to a sequence of four coupled equations which include new objects we may refer to as $\chi_{-,-}$, $\chi_{\uparrow,-}$, and $\chi_{\downarrow,-}$. The number of irreducible particle hole propagators that must be computed likewise is increased by a factor of four. For a very simple version of a one-band Hubbard model, and for a very different purpose, Fulde and Luther[17] carried out an equivalent procedure many years ago. In what follows, we provide a summary of key steps along with expressions for the final set of equations.

To generate the equation of motion, we need the commutator of the operator $S_{\mu\nu}^{+}(l,l')=c_{l\mu\uparrow}^{\dagger}c_{l'\nu\downarrow}$ with the Hamiltonian. One finds

$$[S_{\mu\nu}^{+}(l,l'),H_{SO}]=\frac{1}{2}\sum_{\eta}\{\lambda_{l'}L_{\nu\eta}^{+}c_{l\mu\uparrow}^{\dagger}c_{l'\eta\uparrow}-\lambda_{l}L_{\eta\mu}^{+}c_{l\eta\downarrow}^{\dagger}c_{l'\nu\downarrow}+\lambda_{l'}L_{\nu\eta}^{z}c_{l\mu\uparrow}^{\dagger}c_{l'\eta\downarrow}-\lambda_{l}L_{\eta\mu}^{z}c_{l\eta\uparrow}^{\dagger}c_{l'\nu\downarrow}\}.\qquad(3)$$

The last two terms on the right-hand side of Eq. (3) lead to terms in the equation of motion which involve $\chi_{+,-}$ whereas the first two terms couple us to the entities $\chi_{\uparrow,-}$ and $\chi_{\downarrow,-}$. When we write down the commutator of these new correlation functions with the spin-orbit Hamiltonian, we are led to terms which couple into the function $\chi_{-,-}$ which is formed from the commutator of two S^{-} operators. In the absence of spin-orbit coupling, a consequence of spin-rotation invariance of the Hamiltonian is that the three new functions just encountered vanish. But they do not in its presence, and they must be incorporated into the analysis.

One then introduces the influence of the Coulomb interaction into the equation of motion and carries out an RPA decoupling of the resulting terms. The analysis is very lengthy, so here we summarize only the structure that results from this procedure. Definitions of the various quantities that enter are given in the Appendix. We express the equations of motion in terms of a 4×4 matrix structure, where in schematic notation we let $\chi^{(1)}=\chi_{+,-}$, $\chi^{(2)}=\chi_{\uparrow,-}$, $\chi^{(3)}=\chi_{\downarrow,-}$, and $\chi^{(4)}=\chi_{-,-}$. The four coupled equations then have the form

$$\Omega\chi^{(s)}=A^{(s)}+\sum_{s'}(B^{ss'}+\widetilde{B}^{ss'})\chi^{(s')}.\qquad(4)$$

Each quantity in Eq. (4) has attached to it four orbital indices and four site indices. To be explicit, $\chi^{(2)}=\chi_{\uparrow,-}$ which enters Eq. (4) is formed from the commutator of the operator $c_{l\mu\uparrow}^{\dagger}c_{l'\nu\uparrow}$ with $c_{m\mu'\downarrow}^{\dagger}c_{m'\nu'\uparrow}$ and in full we denote this quantity as $\chi_{\mu\nu;\mu'\nu'}^{(2)}(ll';mm')$. The site indices label the planes in the film, and we suppress reference to Ω and $\vec{Q}_{\parallel}$. The products on the right-hand side of Eq. (4) are matrix multiplications that involve these various indices. For instance, the object $\Sigma_{s'}B^{ss'}\chi^{(s')}$ is labeled by four orbital and four site indices so

$$[B^{ss'}\chi^{(s')}]_{\mu\nu,\mu'\nu'}(ll';mm')=\sum_{\gamma\delta}\sum_{nn'}B_{\mu\nu,\gamma\delta}^{ss'}(ll';nn')\chi_{\gamma\delta,\mu'\nu'}^{(s')}(nn';mm').\qquad(5)$$

One proceeds by writing Eq. (4) in terms of the dynamic susceptibilities that characterize the noninteracting system.

These, referred to also as the irreducible particle-hole propagators, are generated by evaluating the commutators which enter into the definition of $\chi^{(s)}$ in the noninteracting ground state. These objects, denoted by $\chi^{(0s)}$ obey a structure similar to Eq. (4),

$$\Omega\chi^{(0s)} = A^{(s)} + \sum_{s'} B^{ss'}\chi^{(0s')}. \tag{6}$$

It is then possible to relate $\chi^{(s)}$ to $\chi^{(0s)}$ through the relation, using four vector notation,

$$\vec{\chi}(\Omega) = \vec{\chi}^{(0)}(\Omega) + (\Omega - B)^{-1}\tilde{B}\vec{\chi}(\Omega). \tag{7}$$

The matrix structure $\Gamma \equiv (\Omega - B)^{-1}$ may be generated from the definition of B, which may be obtained from the equation of motion of the noninteracting susceptibility, Eq. (6). Then $\tilde{B}$ follows from the equation of motion of the full susceptibility, as generated in the RPA. One may solve Eq. (7)

$$\vec{\chi}(\Omega) = [I - (\Omega - B)^{-1}\bar{B}]^{-1}\vec{\chi}^{(0)}(\Omega), \tag{8}$$

so our basic task is to compute the noninteracting susceptibility matrix $\vec{\chi}^{(0)}$ and then carry out the matrix inversion operation displayed in Eq. (8). For this we require the single-particle Green's functions (SPGFs) associated with our approach.

To generate the SPGFs, we setup an effective single-particle Hamiltonian H_{sp} by introducing a mean-field approximation for the Coulomb interaction. The general structure of the single-particle Hamiltonian is

$$\begin{aligned} H_{sp} = &\sum_{ij}\sum_{\mu\nu\sigma}\tilde{T}_{ij}^{\mu\nu\sigma}c^{\dagger}_{i\mu\sigma}c_{j\nu\sigma} \\ &+ \sum_{i}\sum_{\mu\nu}\{\alpha^{*}_{i;\mu\nu}c^{\dagger}_{i\mu\downarrow}c_{i\nu\uparrow} + \alpha_{i;\mu\nu}c^{\dagger}_{i\mu\uparrow}c_{i\nu\downarrow}\}, \end{aligned} \tag{9}$$

where the effective hopping integral $\tilde{T}_{ij}^{\mu\nu\sigma}$ contains the spin diagonal portion of the spin-orbit interaction, along with the mean-field contributions from the Coulomb interaction. The form we use for the latter is stated below. The coefficients in the spin-flip terms are given by

$$\alpha_{i;\mu\nu} = \lambda_i L^{-}_{\mu\nu} - \sum_{\eta\gamma} U_{i;\eta\mu,\nu\gamma}\langle c^{\dagger}_{i\eta\downarrow}c_{i\gamma\uparrow}\rangle. \tag{10}$$

We then have the eigenvalue equation that generates the single-particle eigenvalues and eigenfunctions in the form $H_{sp}|\phi_s\rangle = E_s|\phi_s\rangle$; we can write this in the explicit form

$$\begin{aligned} &\sum_{l}\sum_{\eta\sigma'}[\delta_{\sigma\sigma'}\tilde{T}_{il}^{\mu\eta\sigma'} + \delta_{il}(\delta_{\sigma'\downarrow}\delta_{\sigma\uparrow}\alpha^{*}_{l;\mu\eta} + \delta_{\sigma'\uparrow}\delta_{\sigma\downarrow}\alpha_{l;\mu\eta})] \\ &\quad \times\langle l\eta\sigma'|\phi_s\rangle = E_s\langle i\mu\sigma|\phi_s\rangle. \end{aligned} \tag{11}$$

The single-particle Green's function may be expressed in terms of the quantities that enter Eq. (11). We have for this object the definition

$$G_{i\mu\sigma;j\nu\sigma'}(t) = -i\theta(t)\langle\{c_{i\mu\sigma}(t), c^{\dagger}_{j\nu\sigma'}(0)\}\rangle \tag{12}$$

and one has the representation

$$G_{i\mu\sigma;j\nu\sigma'}(\Omega) = \sum_{s}\frac{\langle i\mu\sigma|\phi_s\rangle\langle\phi_s|j\nu\sigma'\rangle}{\Omega - E_s + i\eta}. \tag{13}$$

These functions may be constructed directly from their equations of motion, which read, after Fourier transforming with respect to time,

$$\begin{aligned} &-\sum_{l}\sum_{\eta\sigma''}[\delta_{\sigma\sigma''}\tilde{T}_{il}^{\mu\eta\sigma''} + \delta_{il}(\delta_{\sigma''\downarrow}\delta_{\sigma\uparrow}\alpha^{*}_{l;\mu\eta} + \delta_{\sigma''\uparrow}\delta_{\sigma\downarrow}\alpha_{l;\mu\eta})] \\ &\quad \times G_{l\eta\sigma'';j\nu\sigma'} + \Omega G_{i\mu\sigma;j\nu\sigma'} = \delta_{\sigma\sigma'}\delta_{\mu\nu}\delta_{ij}. \end{aligned} \tag{14}$$

For the case where the substrate is semi-infinite, our means of generating a numerical solution to the hierarchy of equations stated in Eq. (14) has been discussed earlier. What remains is to describe how the Coulomb interaction enters the effective hopping integrals $\tilde{T}_{ij}^{\mu\nu\sigma}$ that appear in Eqs. (9), (11), and (14).

There are, of course, a large number of Coulomb matrix elements in the original Hamiltonian, even if the Coulomb interactions are confined to within the 3*d* shell. Through the use of group theory,[18,19] the complete set of Coulomb matrix elements may be expressed in terms of three parameters. These are given in Table I of the first cited paper in Ref. 5. In subsequent work, we have found that a much simpler structure[20] nicely reproduces results obtained with the full three parameter form. We use the simpler one parameter form here, for which $U_{i;\mu\nu,\mu'\nu'} = U_i\delta_{\mu\nu'}\delta_{\mu'\nu}$. Then in the mean-field approximation, the Coulomb contribution to the single-particle Hamiltonian assumes the form

$$H_{sp}^{(C)} = -\sum_{i}\frac{U_i m_i}{2}\sum_{\mu}(c^{\dagger}_{i\mu\uparrow}c_{i\mu\uparrow} - c^{\dagger}_{i\mu\downarrow}c_{i\mu\downarrow}). \tag{15}$$

Here m_i is the magnitude of the moment on site i. The Coulomb interactions U_i are nonzero only within the ultrathin ferromagnet and the moments m_i, determined self-consistently, vary from layer to layer when we consider multilayer ferromagnetic films.

It should be noted that when the Ansatz just described is employed in Eq. (10), the term from the Coulomb interaction on the right-hand side becomes proportional to the transverse component of the moment located on site i and this vanishes identically. Thus, despite the complexity introduced by the spin-orbit coupling, when the simple one parameter Ansatz for the Coulomb matrix elements is employed, one needs no parameters beyond the moment on each layer in the self-consistent loops that describe the ground state. In the present context, this is an extraordinarily large savings in computational labor, and this will allow us to address very large systems in the future. It is the case that certain off-diagonal elements such as $\langle c^{\dagger}_{m\mu'\downarrow}c_{l'\nu\uparrow}\rangle$ appear in the quantities defined in the Appendix. Notice, for example, the expressions in Eq. (A1). Once the ground-state single-particle Green's functions are determined, such expectation values are readily computed.

III. RESULTS AND DISCUSSION

In earlier studies of Fe layers on W(110),[21,22] as noted above, the electronic structure was generated through use of tight-binding parameters obtained from bulk electronic-structure calculations. These calculations generate effective exchange interactions comparable in magnitude to those found in the bulk transition metals,[22] with the consequence that for both monolayer Fe and bilayer Fe on W(110) the large wave-vector spin waves generated by theory are very much stiffer than found experimentally[23,24] though it should be noted that for the bilayer, the calculated value of the spin-wave exchange stiffness is in excellent accord with the data.[25] Subsequent calculations which construct the spin-wave dispersion relation from adiabatic theory based on calculations of effective exchange integrals also generate spin waves for the monolayer substantially stiffer than found experimentally,[10] though they are softer than in our earlier work by a factor of two or so. We remark that it has been suggested that the remarkably soft spin waves found experimentally may have origin in carbon contamination of the monolayer and bilayer.[22] We remark here that this can be introduced during the SPEELS measurement. We note that the magnetic properties of Fe monolayers grown on carbon free W(110) (Ref. 26) differ dramatically from those grown on surfaces now known to be contaminated by carbon.[27] In the former case, the domain walls have a thickness of 2.15 nm (Ref. 26) whereas in the latter circumstance very narrow walls with thickness bounded from above by 0.6 nm are found.[27] This suggests that the strength of the effective exchange is very different in the two cases with stiffer exchange in the carbon-free samples.

The considerations of the previous paragraph have motivated us to carry out a series of studies of the effective exchange in the Fe monolayer on W(110) within the framework of three different electronic structure calculations. We find that although all three give local density of states that are very similar, along with very similar energy bands when these are examined, the intersite exchange interactions vary substantially. First, we have employed the parameter set used earlier that is based on bulk electronic structures[21,22] in new calculations we call case A. In case B, we have employed an approach very similar to that used in Ref. 10, though in what follows our calculation of effective exchange integrals is nonrelativistic. This is the KKR-GF method,[28] which employs the atomic sphere approximation and makes use of the Dyson equation $G=g+gVG$ as given in matrix notation. This allows us to calculate the Green's function G of an arbitrary complex system given the perturbing potential V and the Green's function g of a reference unperturbed system. Within the local spin-density approximation (LSDA),[29] we consider a slab of five monolayers of W with the experimental lattice constant on top of which an Fe monolayer is deposited and relaxed by −12.9% (Ref. 10) with respect to the W interlayer distance. Angular momenta up to $l_{\max}=3$ were included in the Green's functions with a k mesh of 6400 points in the full two-dimensional Brillouin zone. The effective exchange interactions were calculated within the approximation of infinitesimal rotations[30] that allows one to use the magnetic force theorem. This states that the energy change due to infinitesimal rotations in the moment directions can be calculated through the Kohn-Sham eigenvalues.

Method C is the real-space linear-muffin-tin-orbital approach as implemented, also, in the atomic sphere approximation (RS-LMTO-ASA).[31–35] Due to its linear scaling, this method allows one to address the electronic structure of systems with a large number of atoms for which the basic eigenvalue problem is solved in real space using the Haydock recursion method. The Fe overlayer on the W(110) substrate was simulated by a large bcc slab which contained ~6800 atoms, arranged in 12 atomic planes parallel to the (110) surface, with the experimental lattice parameter of bulk W. One empty sphere overlayer is included and self-consistent potential parameters were obtained for the empty-sphere overlayer, the Fe monolayer, and the three W layers underneath using LSDA.[36] For deeper W layers we use bulk potential. Nine orbitals per site (the five 3*d* and four *sp* complex) were used to describe the Fe valence band and the empty sphere overlayer, and for W the fully occupied 4*f* orbitals were also included in the core. To evaluate the orbital moments we use a scalar relativistic approach and include a spin-orbit coupling term $\lambda\vec{L}\cdot\vec{S}$ at each variational step.[37] In the recursion method the continued fraction has been terminated after 30 recursion levels with the Beer-Pettifor terminator.[38,39] Tight-binding parameters are extracted from the KKR calculations by fitting the energy bands of the unsupported monolayer to a nine-orbital tight-binding model. The Fe/W hopping is adjusted to give a reasonable value of magnetic moment. The parameters from the RS-LMTO-ASA calculation are extracted according to the procedure given in Ref. 40. The TB parameters so obtained are inserted into our semiempirical scheme and this allows us to generate the noninteracting susceptibilities which enter our full RPA description of the response of the structure.

In order to compare the electronic structures generated by the approaches just described, we turn our attention to the local density of states for the majority and minority spins in the adsorbed Fe monolayer. These are summarized in Fig. 1.

The local densities of states (LDOSs) generated by the three sets of TB parameters have approximately the same overall features, as we see from Fig. 1. The main differences appear in the majority-spin band, which overlaps the 5*d* states in the W substrate over a larger energy range than the minority band. This is also true if we compare the LDOS generated by the tight-binding parameters extracted from the KKR electronic structure to the LDOS obtained directly from the KKR calculations [red dashed line in Fig. 1(b)]. The Fe-W hopping parameters are indeed the least accurate portion of our parametrization scheme. In case A we just used the Fe-Fe bulk parameters to describe the Fe-W hopping. In case B we extracted TB parameters for Fe by fitting a KKR calculation of an unsupported Fe monolayer with a lattice parameter matching that of the W substrate. For the Fe-W hopping we used the Fe parameters obtained from the fitting, scaled to mimic the Fe-W distance relaxation. The relaxation parameter was chosen to give the correct spin magnetic moment for the adsorbed Fe monolayer. In case C all parameters were directly provided by the RS-LMTO-ASA code, but in the DFT calculations the Fe-W distance was assumed to be equal to the distance between W layers. Thus, the main difference between cases B and C is the treatment of the mixing between Fe and W states and this is expected to affect more strongly the states that occupy the same energy range.

As noted above, while the local density of states provided by the three approaches to the electronic structure are quite

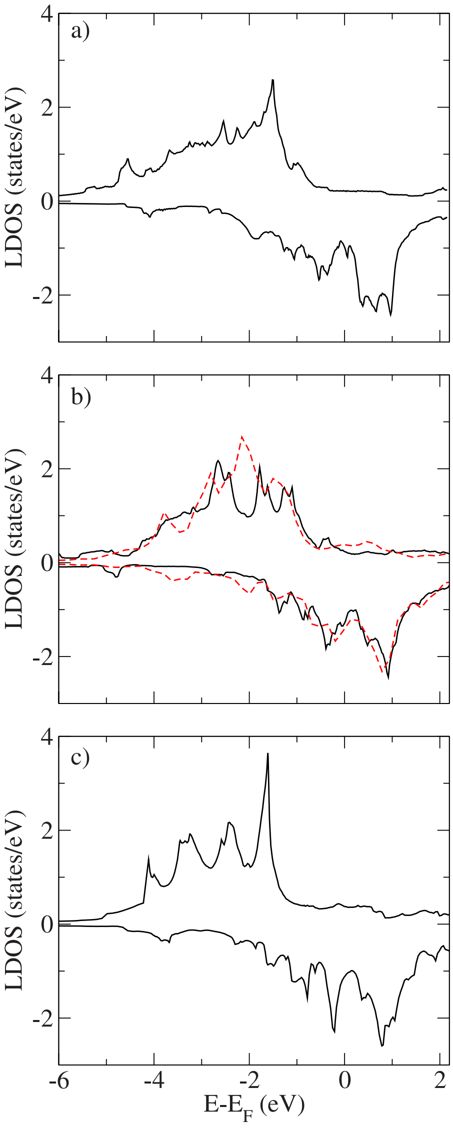

FIG. 1. (Color online) For the Fe monolayer adsorbed on W(110), we show the local density of states in the Fe monolayer. The majority-spin density of states is shown positive and the minority-spin density of states is negative. The zero of energy is at the Fermi energy. In (a), bulk electronic structure parameters are used as in the second of the two papers cited in Ref. 5 (case A). In (b), we have the density of states generated by method B. The black curve is found by fitting the KKR electronic energy band structure to tight-binding parameters as described in the text and the red dashed curve is calculated directly from the KKR calculation. In (c) we have the local density of states generated by method C.

similar as we see from Fig. 1 (and the same is true of the electronic energy bands themselves if these are examined), the exchange interactions differ substantially for the three cases. For the first, second, and third neighbors we have (in meV) 42.5, 3.72, and 0.46 for model A, 28.7, −7.87, and 0.31 for model B, and 11.23, −7.31, and 0.22 for model C. The authors of Ref. 10 find 10.84, −3.34, and 3.64 for these exchange integrals.

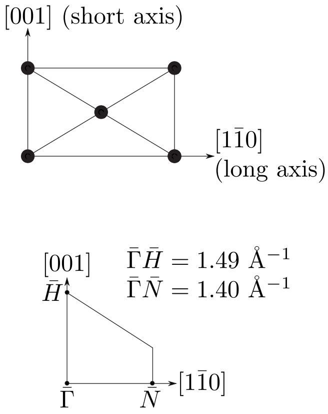

FIG. 2. Schematic representation of in-plane lattice points and two-dimensional Brillouin zone geometry. The easy axis for the monolayer is parallel to [1$\bar{1}$0] in both cases B and C. For the bilayer, the easy axis is perpendicular to the film in case B and parallel to [1$\bar{1}$0] in case C.

We now turn to our studies of spin excitations in the Fe monolayer and Fe bilayer on W(110) within the framework of the electronic structure generated through use of the approach in case C. We will discuss the influence of spin-orbit coupling on both the transverse wave-vector-dependent susceptibility through study of the spectral density function $A(\vec{Q}_\parallel,\Omega;l_\perp)=-\mathrm{Im}\{\chi_{+,-}(\vec{Q}_\parallel,\Omega;l_\perp)\}$ discussed in Sec. II. This function, for fixed wave vector $\vec{Q}_\parallel$, when considered as a function of frequency Ω, describes the frequency spectrum of the fluctuations of wave vector $\vec{Q}_\parallel$ of the transverse magnetic moment in layer $l_\perp$ as noted above. In the frequency regime where spin waves are encountered, this function is closely related to (but not identical to) the response function probed in a SPEELS measurement.

In Fig. 2 we show, for reference, a schematic representation of the in-plane lattice directions and of the two-dimensional Brillouin zone. In Fig. 3, for the Fe monolayer on W(110), we show the spectral density function calculated for three values of $|\vec{Q}_\parallel|$, for propagation perpendicular to the magnetization. Thus, the wave vector is directed along the short axis in the surface. This is the direction probed in SPEELS studies of the Fe monolayer on this surface.[24] In each figure, we show three curves. The green dashed curve is calculated with spin-orbit coupling set to zero. We show only a single curve for this case, because the spectral density is identical for the two directions of propagation perpendicular to the magnetization, $+\vec{Q}_\parallel$ and $-\vec{Q}_\parallel$. When spin-orbit coupling is switched on, for the two directions just mentioned the response function is very different, as we see from the red and black curves in the various panels. These spin-wave frequencies, deduced from the peak in the response functions as discussed in Sec. I, differ for the two directions of propagation, and also note that the peak intensities and linewidths differ as well. It is the absence of both time-reversal symmetry and reflection symmetry which renders $+\vec{Q}_\parallel$ and $-\vec{Q}_\parallel$ inequivalent for this direction of propagation. The system senses this breakdown of symmetry through the spin-orbit interaction. If one considers propagation parallel to the magnetization, the asymmetries displayed in Fig. 3 are absent. The reason is that for this direction of propagation, reflection in the plane that is perpendicular to both the magnetization

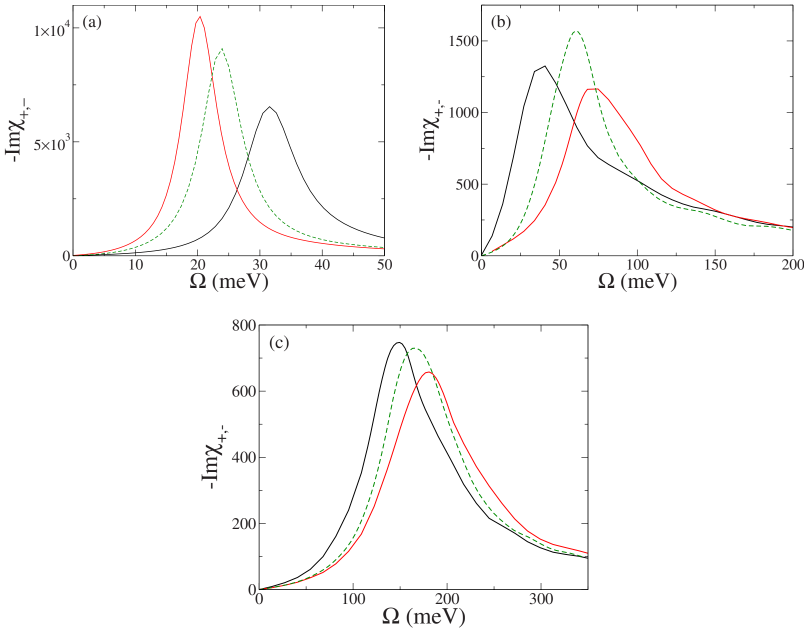

FIG. 3. (Color online) The spectral density functions $A(\vec{Q}_\parallel,\Omega;l_\perp)$ evaluated in the Fe monolayer for three values of the wave vector in the direction perpendicular to the magnetization. We have (a) $|\vec{Q}_\parallel|=0.4$ Å^{-1}, (b) $|\vec{Q}_\parallel|=1.0$ Å^{-1}, and (c) $|\vec{Q}_\parallel|=1.4$ Å^{-1}. The green curve (dashed) is calculated with spin-orbit coupling set to zero; the spectral density here is independent of the sign of $\vec{Q}_\parallel$. The red and black curves are calculated with spin-orbit coupling turned on. Now we see asymmetries for propagation perpendicular to the magnetization with the red curve $\vec{Q}_\parallel$ directed from left to right and the black curve from right to left.

and the surface is a good symmetry operation of the system, but takes $+\vec{Q}_\parallel$ into $-\vec{Q}_\parallel$ thus rendering the two directions equivalent. Recall, of course, that the magnetization is a pseudovector in regard to reflections. Notice how very broad the curves are for large wave vectors; the lifetime of the spin waves is very short indeed.

As discussed in Sec. I, we may construct a spin-wave dispersion curve by plotting the maxima in spectral-density plots such as those illustrated in Fig. 3 as a function of wave vector. We show dispersion relations constructed in this manner in Fig. 4 with spin-orbit coupling both present and absent. In Fig. 4(a), and for propagation perpendicular to the magnetization we show the dispersion curve so obtained for wave vectors throughout the surface Brillouin zone and in Fig. 4(b) we show its behavior for small wave vectors.

Let us first consider Fig. 4(a). Here the dispersion curve extends throughout the two-dimensional Brillouin zone. At the zone boundary, quite clearly the slope of the dispersion curve does not vanish. In this direction of propagation, the nature of the point at the zone boundary does not require the slope to vanish. What is most striking, clearly, is the anomaly in the vicinity of 1 Å^{-1}. This feature is evident in the calculation with spin-orbit coupling absent and for positive values of the wave vector the feature becomes much more dramatic when spin-orbit coupling is switched on. Anomalies rather similar to those in the black curve in Fig. 4(a) appear in the green dispersion curve found in Fig. 3 of Ref. 10, though these authors did not continue their calculation much beyond the 1 Å^{-1} regime. Our spin waves are very much softer than theirs in this spectral region, notice.

In Fig. 4(b), again with spin-orbit coupling switched on and off, we show an expanded view of the dispersion curve for small wave vectors. With spin-orbit interaction switched off, at zero wave vector we see a zero-frequency spin-wave mode, as required by the Goldstone theorem when the underlying Hamiltonian is form invariant under spin rotation. The curve is also symmetrical and is accurately fitted by the form $\Omega(\vec{Q}_\parallel)=149Q_\parallel^2$ (meV), with the wave vector in per angstrom, whereas with spin-orbit coupling turned on the dispersion relation is fitted by $\Omega(\vec{Q}_\parallel)=3.4+11.8Q_\parallel+143Q_\parallel^2$ (meV). Spin-orbit coupling introduces an anisotropy gap at $Q_\parallel=0$ and most striking is the term linear in wave vector. This has its origin in the Dzyaloshinskii-Moriya interaction whose presence, as argued by the authors of Ref. 9, has its origin in the absence of both time-reversal and inversion symmetry, for the adsorbed layer.

At long wavelengths, one may describe spin waves by classical long-wavelength phenomenology. The linear term in the dispersion curve has its origin in a term in the energy density of the spin system of the form

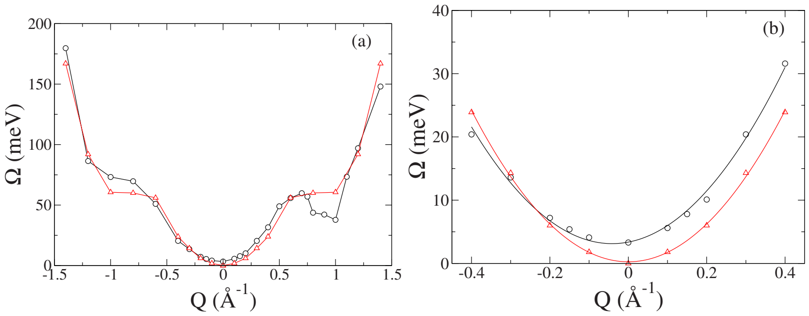

FIG. 4. (Color online) Spin-wave dispersion relations constructed from peaks in the spectral density for the Fe monolayer on W(110). The wave vector is in the direction perpendicular to the magnetization. The red curve is constructed in the absence of spin-orbit coupling, which is included in the black curve. Panel (b) is a zoom of panel (a) at the small wave-vector region.

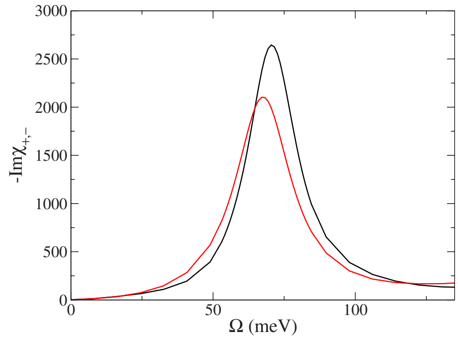

FIG. 5. (Color online) The spectral density in the outermost layer, in the acoustic spin-wave regime, for wave vectors of $Q_{\parallel}=+0.5$ Å^{-1} (black curve) and $Q_{\parallel}=-0.5$ Å^{-1} (red curve). Model C has been used for the calculation. In the ground state, the magnetization lies in plane along the long axis.

$$V_{\mathrm{DM}}=-\Gamma\int dxdzS_y(x,z)\frac{\partial S_x(x,z)}{\partial x}. \tag{16}$$

Here $S_{\alpha}(x,z)$ is a spin density, the xz plane is parallel to the surface, and the magnetization is parallel to the z direction.

One interesting feature of the spin-wave mode whose dispersion relation is illustrated in Fig. 4(b) is that at $Q_{\parallel}=0$, the mode has a finite group velocity. The fit to the dispersion curve gives this group velocity to be $\frac{\partial\Omega(\vec{Q}_{\parallel})}{\partial Q_{\parallel}}\approx 2\times 10^5$ cm/s, which is in the range of acoustic phonon group velocities.

We turn now to our calculations of spin waves and the response functions for the Fe bilayer on W(110). Let us first note that experimentally the orientation of the magnetization in the bilayer appears to be dependent on the surface upon which the bilayer is grown. For instance, when the bilayer is on the stepped W(110) surface, it is magnetized perpendicular to the surface,[27] a result in agreement with *ab initio* calculations of the anisotropy realized in the epitaxial bilayer.[41] However, in the SPEELS studies of spin excitations in the bilayer[11,24] the magnetization is in plane. In our calculations, we find for model B the magnetization is perpendicular to the surface whereas in model C it lies in plane, along the long axis very much as in the SPEELS experiments. The anisotropy in the bilayer is not particularly large, on the order of 0.5 meV/Fe atom, and one sees from these results that it is a property quite sensitive to the details of the electronic structure. The fact that model B and model C give the two different stable orientations of the magnetization allows us to explore spin excitations for the two different orientations of the magnetization.

We first turn our attention to the case where the magnetization lies in plane. The bilayer has two spin-wave modes, an acoustic mode for which the magnetization in the two planes precesses in phase and an optical mode for which they precess 180° out of phase. In Fig. 5, we show calculations of the dynamic susceptibility in the frequency range of the acoustic mode for two values of the wave vector, $Q_{\parallel}=+0.5$ Å^{-1} and $Q_{\parallel}=-0.5$ Å^{-1}. A spin-orbit-induced left-right asymmetry is clearly evident both in the peak frequency and the height of the feature. Very recently, beautiful measurements of spin-orbit asymmetries in the Fe bilayer have appeared,[11] and the results of our Fig. 5 are to be compared with Fig. 3 of Ref. 11. Theory and experiment are very similar, both in regard to the intensity asymmetry and also the spin-orbit-induced frequency shift, though our calculated spin-wave frequencies are a little stiffer than those found experimentally.

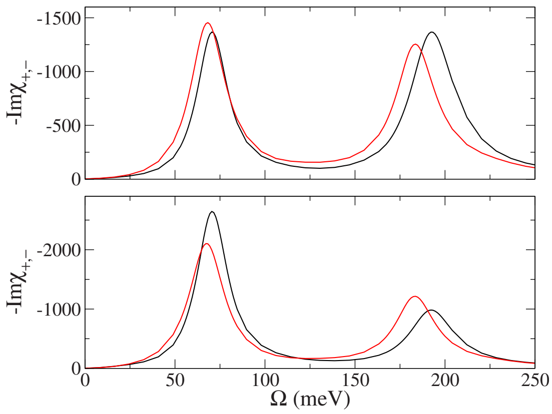

FIG. 6. (Color online) For the wave vector $Q_{\parallel}=0.5$ Å^{-1} we show the spectral densities in the innermost Fe layer (upper panel) and in the outermost layer (lower panel) for the Fe bilayer on W(110). The figure includes the optical spin-wave feature. As in Fig. 5, the black curve is calculated for $Q_{\parallel}$ positive and the red curves are for $Q_{\parallel}$ negative. The calculations employ model C.

As remarked above, in Fig. 5 we show only the acoustical spin-wave mode frequency regime. In Fig. 6, for the spectral densities in the innermost layer (upper panel) and the outermost layer (lower panel) we show the spectral densities for the entire spin-wave regime, including the region where the optical spin wave is found. It is clear that the spin-orbit-induced frequency shifts are largest for the optical mode which unfortunately is not observed in the experiments.[11]

In Fig. 7 for a sequence of wave vectors, all chosen positive, we show a sequence of spectra calculated for the entire frequency range so both the acoustic and optical spin-wave feature are displayed. The black curves show the spectral density of the innermost Fe layer and the red curves are for the outer layer. The optical spin-wave mode, not evident in the data, shows clearly in these figures. Notice that for wave vectors greater than 1 Å^{-1} the acoustical mode is localized in the outer layer and the optical mode is localized on the inner layer. The optical mode is very much broader than the acoustical mode at large wave vectors, by virtue of the strong coupling to the electron-hole pairs in the W 5*d* bands.

An interesting issue is the absence of the optical mode from the SPEELS spectra reported in Refs. 11 and 24. We note that these spectra are taken with only two beam energies, 4 and 6.75 eV. At such very low energies, the beam electron will sample both Fe layers, so the SPEELS signal will be a coherent superposition of electron waves backscattered from each layer; the excitation process involves coherent excitation of both layers by the incident electron. As a consequence of the 180° phase difference in spin motions associated with the two modes it is quite possible, indeed even probable, that for energies where the acoustical mode is strong the intensity of the optical mode is weak, by virtue of quantum interference effects in the excitation scattering amplitude. In earlier studies of surface phonons, it is well docu-

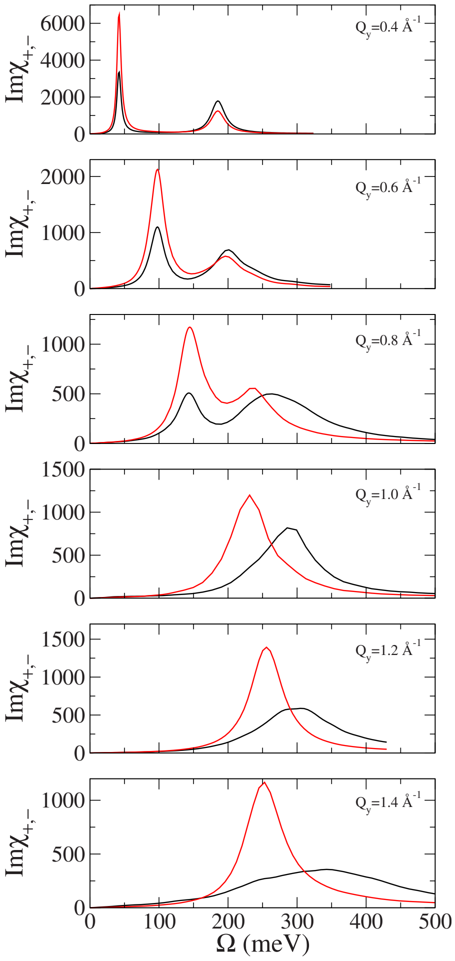

FIG. 7. (Color online) For the Fe bilayer and for several values of the wave vector (all positive), we show the spectral density functions for the innermost layer adjacent to the substrate (black curve) and those for the outer layer of the film. The calculations employ model C.

mented that on surfaces where two surface phonons of different polarization exist for the same wave vector, one can be silent and one active in electron-loss spectroscopy.[42] It would require a full multiple scattering analysis of the spin-wave excitation process to explore this theoretically. While earlier[43] calculations that address SPEELS excitation of spin waves described by the Heisenberg model could be adapted for this purpose, in principle, a problem is that at such low-beam energies it is necessary to take due account of image potential effects to obtain meaningful results.[44] This is very difficult to do without considerable information on the electron reflectivity of the surface.[44] It would be of great interest to see experimental SPEELS studies of the Fe bilayer with a wider range of beam energies to search for the optical mode, if this were possible.

In Fig. 8, we show dispersion curves for the optical and acoustic spin-wave branches for the bilayer. The magnetization lies in plane, and one can see that on the scale of this figure, the spin-orbit effects on the dispersion curve are rather modest compared to those in the monolayer. For small wave vectors, with spin-orbit coupling present, the dispersion curve of the acoustic spin-wave branch is fitted by the form $\Omega(Q_\parallel)=0.49-0.85Q_\parallel+244Q_\parallel^2$ (meV) so at long wavelengths the influence of the Dzyaloshinskii-Moriya interaction is more than one order of magnitude smaller than it is in the monolayer.

If the magnetization is perpendicular to the surface then symmetry considerations show that there are no left/right asymmetries in the spin-wave propagation characteristics. One may see this as follows. Consider a wave vector $\vec{Q}_\parallel$ in the plane of the surface, which is perpendicular to the magnetization. The reflection R in the plane perpendicular to the surface and which contains the magnetization simultaneously changes the sign of wave vector and the magnetization. If this is followed by the time-reversal operation T then $\vec{Q}_\parallel$ remains reversed in sign but the magnetization changes back to its original orientation. Thus the product RT leaves the system invariant but transforms $\vec{Q}_\parallel$ into $-\vec{Q}_\parallel$. The two propagation directions are then equivalent.

We illustrate this in Fig. 9 where, for $Q_\parallel=0.6$ Å^{-1}, where it is shown that the spectral densities calculated for the two directions of propagation are identical with spin-orbit coupling switched on. Model B, in which the magnetization is perpendicular to the surface, has been used in these calculations. The spectral densities calculated for the two signs of $Q_\parallel$ cannot be distinguished to within the numerical precision we use.

IV. CONCLUDING REMARKS

We have developed the formalism which allows one to include the influence of spin-orbit coupling on the spin excitations of ultrathin ferromagnets on semi-infinite metallic substrates. Our approach allows us to calculate the full dynamic susceptibility of the system, so as illustrated by the calculations presented in Sec. III we can examine the influence of spin-orbit coupling on the linewidth (or lifetime) of

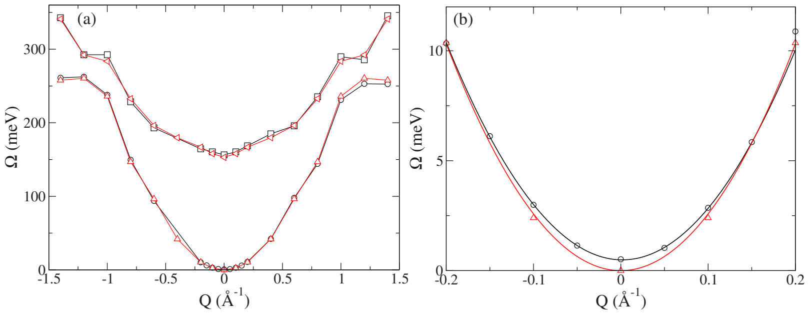

FIG. 8. (Color online) For the Fe bilayer with magnetization in plane we show, in panel (a), the spin-wave dispersion curves calculated with spin-orbit coupling (black symbols) and without spin-orbit coupling (red symbols). Panel (b) is a zoom of panel (a) at the small wave-vector region, together with fittings to quadratic functions (see text). Model C has been employed for these calculations.

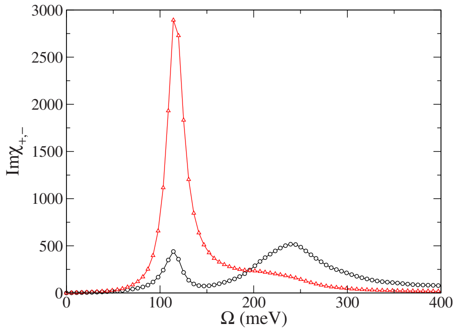

FIG. 9. (Color online) For the bilayer and the case where the magnetization is perpendicular to the surface (model B), and for $Q_{\parallel}=0.6$ Å^{-1}, we show spectral density function calculated for positive values of $Q_{\parallel}$ (continuous lines) and negative values of $Q_{\parallel}$ (symbols). The black curve is the spectral density for the inner layer and the red curve is the outermost Fe layer.

spin excitations, along with their oscillator strength. As in previous work, we can then construct effective dispersion curves by following peaks in the spectral density as a function of wave vector without resort to calculations of large numbers of very small distant-neighbor exchange interactions. The results presented in Fig. 5 are very similar to the experimental data reported in Ref. 11, as discussed above, though we see that in the bilayer the influence of the Dzyaloshinskii-Moriya interaction is considerably more modest than in the monolayer.

We will be exploring other issues in the near future. One interest in our minds is the influence of spin-orbit coupling on the spin pumping contributions to the ferromagnetic resonance linewidth, as observed in ferromagnetic resonance (FMR) studies of ultrathin films.[45] It has been shown earlier[14] that the methodology employed in the present paper (without spin-orbit coupling included) can be applied to the description of the spin pumping contribution to the FMR linewidth, and, in fact, an excellent quantitative account of the data on the Fe/Au(100) system was obtained. It is possible that for films grown on 4*d* and 5*d* substrates that spin-orbit coupling can influence the spin pumping relaxation rate substantially. This will require calculations directed toward much thicker films than explored here. The formalism we have developed and described in the present paper will allow such studies in the future.

ACKNOWLEDGMENTS

This research was supported by the U. S. Department of Energy through Grant No. DE-FG03-84ER-45083. S.L. wishes to thank the Alexander von Humboldt Foundation for support. A.T.C. and R.B.M. acknowledge support from CNPq and FAPERJ and A.B.K. was supported also by the CNPq, Brazil.

APPENDIX

In this appendix we provide explicit expressions for the various quantities which enter the equations displayed in Sec. II. While these expressions are unfortunately lengthy, it will be useful for them to be given in full.

$$\begin{aligned}
A^{(1)}_{\mu\nu,\mu'\nu'}(ll';mm') &= \delta_{l'm}\delta_{\nu\mu'}\langle c^{\dagger}_{l\mu\uparrow}c_{m'\nu'\uparrow}\rangle \\
&\quad - \delta_{lm'}\delta_{\mu\nu'}\langle c^{\dagger}_{m\mu'\downarrow}c_{l'\nu\downarrow}\rangle \\
A^{(2)}_{\mu\nu,\mu'\nu'}(ll';mm') &= -\,\delta_{lm'}\delta_{\mu\nu'}\langle c^{\dagger}_{m\mu\downarrow}c_{l'\nu\uparrow}\rangle \\
A^{(3)}_{\mu\nu,\mu'\nu'}(ll';mm') &= \delta_{l'm}\delta_{\nu\mu'}\langle c^{\dagger}_{l\mu\downarrow}c_{m'\nu'\uparrow}\rangle \\
A^{(4)}_{\mu\nu,\mu'\nu'}(ll';mm') &= 0
\end{aligned}\tag{A1}$$

The various expectation values in the equations above and those displayed below are calculated from the single-particle Green's functions once the self-consistent ground-state parameters are determined. Then

$$\begin{aligned}
\widetilde{B}^{11}_{\mu\nu,\mu'\nu'}(ll';mm') &= \sum_{\eta}\,(U_{l;\mu'\eta,\mu\nu'}\langle c^{\dagger}_{l\eta\downarrow}c_{l'\nu\downarrow}\rangle\delta_{lm}\delta_{lm'} \\
&\quad - U_{l';\mu'\nu,\eta\nu'}\langle c^{\dagger}_{l\mu\uparrow}c_{l'\eta\uparrow}\rangle\delta_{l'm}\delta_{l'm'}), \\
\widetilde{B}^{12}_{\mu\nu,\mu'\nu'}(ll';mm') &= \sum_{\eta}\,(U_{l';\mu'\nu,\nu'\eta}\langle c^{\dagger}_{l\mu\uparrow}c_{l'\eta\downarrow}\rangle\delta_{l'm}\delta_{l'm'} \\
&\quad - U_{l;\eta\mu',\mu\nu'}\langle c^{\dagger}_{l\eta\uparrow}c_{l'\nu\downarrow}\rangle\delta_{lm}\delta_{lm'} \\
&\quad + U_{l;\mu'\eta,\mu\nu'}\langle c^{\dagger}_{l\eta\uparrow}c_{l'\nu\downarrow}\rangle\delta_{lm}\delta_{lm'}), \\
\widetilde{B}^{13}_{\mu\nu,\mu'\nu'}(ll';mm') &= \sum_{\eta}\,(U_{l';\mu'\nu,\nu'\eta}\langle c^{\dagger}_{l\mu\uparrow}c_{l'\eta\downarrow}\rangle\delta_{l'm}\delta_{l'm'} \\
&\quad - U_{l;\eta\mu',\mu\nu'}\langle c^{\dagger}_{l\eta\uparrow}c_{l'\nu\downarrow}\rangle\delta_{lm}\delta_{lm'} \\
&\quad - U_{l';\mu'\nu,\eta\nu'}\langle c^{\dagger}_{l\mu\uparrow}c_{l'\eta\downarrow}\rangle\delta_{l'm}\delta_{l'm'}), \\
\widetilde{B}^{14}_{\mu\nu,\mu'\nu'}(ll';mm') &= 0,
\end{aligned}\tag{A2}$$

$$\begin{aligned}
\widetilde{B}^{21}_{\mu\nu,\mu'\nu'}(ll';mm') &= \sum_{\eta}\,U_{l;\mu'\eta,\mu\nu'}\langle c^{\dagger}_{l\eta\downarrow}c_{l'\nu\uparrow}\rangle\delta_{lm}\delta_{lm'}, \\
\widetilde{B}^{22}_{\mu\nu,\mu'\nu'}(ll';mm') &= \sum_{\eta}\,[(U_{l';\mu'\nu,\nu'\eta} - U_{l';\mu'\nu,\eta\nu'}) \\
&\quad \times\langle c^{\dagger}_{l\mu\uparrow}c_{l'\eta\uparrow}\rangle\delta_{l'm}\delta_{l'm'} - (U_{l;\eta\mu',\mu\nu'} \\
&\quad - U_{l;\mu'\eta,\mu\nu'})\langle c^{\dagger}_{l\eta\uparrow}c_{l'\nu\uparrow}\rangle\delta_{lm}\delta_{lm'}], \\
\widetilde{B}^{23}_{\mu\nu,\mu'\nu'}(ll';mm') &= \sum_{\eta}\,(U_{l;\mu'\nu,\nu'\eta}\langle c^{\dagger}_{l\mu\uparrow}c_{l'\eta\uparrow}\rangle\delta_{l'm}\delta_{l'm'} \\
&\quad - U_{l;\eta\mu',\mu\nu'}\langle c^{\dagger}_{l\eta\uparrow}c_{l'\nu\uparrow}\rangle\delta_{lm}\delta_{l'm'}), \\
\widetilde{B}^{24}_{\mu\nu,\mu'\nu'}(ll';mm') &= -\sum_{\eta}\,U_{l';\mu'\nu,\eta\nu'}\langle c^{\dagger}_{l\mu\uparrow}c_{l'\eta\downarrow}\rangle\delta_{l'm}\delta_{l'm'},
\end{aligned}\tag{A3}$$

$$\begin{aligned}
\widetilde{B}^{31}_{\mu\nu,\mu'\nu'}(ll';mm') &= -\sum_{\eta} U_{l';\mu'\nu,\eta\nu'}\langle c^{\dagger}_{l\mu\downarrow}c_{l'\eta\uparrow}\rangle\delta_{l'm}\delta_{l'm'},\\
\widetilde{B}^{32}_{\mu\nu,\mu'\nu'}(ll';mm') &= \sum_{\eta}(U_{l;\mu'\nu,\nu'\eta}\langle c^{\dagger}_{l\mu\downarrow}c_{l'\eta\downarrow}\rangle\delta_{l'm}\delta_{l'm'}\\
&\quad - U_{l;\eta\mu',\mu\nu'}\langle c^{\dagger}_{l\eta\downarrow}c_{l'\nu\downarrow}\rangle\delta_{lm}\delta_{l'm'}),\\
\widetilde{B}^{33}_{\mu\nu,\mu'\nu'}(ll';mm') &= \sum_{\eta}[(U_{l';\mu'\nu,\nu'\eta} - U_{l';\mu'\nu,\eta\nu'})\\
&\quad \times\langle c^{\dagger}_{l\mu\downarrow}c_{l'\eta\downarrow}\rangle\delta_{l'm}\delta_{l'm'} - (U_{l;\eta\mu',\mu\nu'}\\
&\quad - U_{l;\mu'\eta,\mu\nu'})\langle c^{\dagger}_{l\eta\downarrow}c_{l'\nu\downarrow}\rangle\delta_{lm}\delta_{lm'}],\\
\widetilde{B}^{34}_{\mu\nu,\mu'\nu'}(ll';mm') &= \sum_{\eta} U_{l;\mu'\eta,\mu\nu'}\langle c^{\dagger}_{l\eta\uparrow}c_{l'\nu\downarrow}\rangle\delta_{lm}\delta_{lm'},
\end{aligned} \tag{A4}$$

$$\begin{aligned}
\widetilde{B}^{41}_{\mu\nu,\mu'\nu'}(ll';mm') &= 0,\\
\widetilde{B}^{42}_{\mu\nu,\mu'\nu'}(ll';mm') &= \sum_{\eta}(U_{l';\mu'\nu,\nu'\eta}\langle c^{\dagger}_{l\mu\downarrow}c_{l'\eta\uparrow}\rangle\delta_{l'm}\delta_{l'm'}\\
&\quad - U_{l;\eta\mu',\mu\nu'}\langle c^{\dagger}_{l\eta\downarrow}c_{l'\nu\uparrow}\rangle\delta_{lm}\delta_{lm'}\\
&\quad - U_{l';\mu'\nu,\eta\nu'}\langle c^{\dagger}_{l\mu\downarrow}c_{l'\eta\uparrow}\rangle\delta_{l'm}\delta_{l'm'}),\\
\widetilde{B}^{43}_{\mu\nu,\mu'\nu'}(ll';mm') &= \sum_{\eta}(U_{l';\mu'\nu,\nu'\eta}\langle c^{\dagger}_{l\mu\downarrow}c_{l'\eta\uparrow}\rangle\delta_{l'm}\delta_{l'm'}\\
&\quad - U_{l;\eta\mu',\mu\nu'}\langle c^{\dagger}_{l\eta\downarrow}c_{l'\nu\uparrow}\rangle\delta_{lm}\delta_{lm'}\\
&\quad + U_{l;\mu'\eta,\mu\nu'}\langle c^{\dagger}_{l\eta\downarrow}c_{l'\nu\uparrow}\rangle\delta_{lm}\delta_{lm'}),\\
\widetilde{B}^{44}_{\mu\nu,\mu'\nu'}(ll';mm') &= \sum_{\eta}(U_{l;\mu'\eta,\mu\nu'}\langle c^{\dagger}_{l\eta\uparrow}c_{l'\nu\uparrow}\rangle\delta_{lm}\delta_{l'm}\\
&\quad - U_{l';\mu'\nu,\eta\nu'}\langle c^{\dagger}_{l\mu\downarrow}c_{l'\eta\downarrow}\rangle\delta_{l'm}\delta_{l'm'}),
\end{aligned} \tag{A5}$$

$$\begin{aligned}
B^{11}_{\mu\nu,\mu'\nu'}(ll';mm') &= \widetilde{T}^{\nu\nu'\downarrow}_{l'm'}\delta_{lm}\delta_{\mu\mu'} - (\widetilde{T}^{\mu\mu'\uparrow}_{lm})^{*}\delta_{l'm'}\delta_{\nu\nu'},\\
B^{12}_{\mu\nu,\mu'\nu'}(ll';mm') &= \alpha^{*}_{l';\nu'\nu}\delta_{lm}\delta_{l'm'}\delta_{\mu\mu'},\\
B^{13}_{\mu\nu,\mu'\nu'}(ll';mm') &= -\alpha^{*}_{l;\mu\mu'}\delta_{lm}\delta_{l'm'}\delta_{\nu\nu'},\\
B^{14}_{\mu\nu,\mu'\nu'}(ll';mm') &= 0,
\end{aligned} \tag{A6}$$

$$\begin{aligned}
B^{21}_{\mu\nu,\mu'\nu'}(ll';mm') &= \alpha_{l';\nu\nu'}\delta_{lm}\delta_{l'm'}\delta_{\mu\mu'},\\
B^{22}_{\mu\nu,\mu'\nu'}(ll';mm') &= \widetilde{T}^{\nu\nu'\uparrow}_{l'm'}\delta_{lm}\delta_{\mu\mu'} - (\widetilde{T}^{\mu\mu'\uparrow}_{lm})^{*}\delta_{l'm'}\delta_{\nu\nu'},\\
B^{23}_{\mu\nu,\mu'\nu'}(ll';mm') &= 0,\\
B^{24}_{\mu\nu,\mu'\nu'}(ll';mm') &= -\alpha^{*}_{l;\mu\mu'}\delta_{lm}\delta_{l'm'}\delta_{\nu\nu'},
\end{aligned} \tag{A7}$$

$$\begin{aligned}
B^{31}_{\mu\nu,\mu'\nu'}(ll';mm') &= -\alpha_{l;\mu'\mu}\delta_{lm}\delta_{l'm'}\delta_{\nu\nu'},\\
B^{32}_{\mu\nu,\mu'\nu'}(ll';mm') &= 0,\\
B^{33}_{\mu\nu,\mu'\nu'}(ll';mm') &= \widetilde{T}^{\nu\nu'\downarrow}_{l'm'}\delta_{lm}\delta_{\mu\mu'} - (\widetilde{T}^{\mu\mu'\downarrow}_{lm})^{*}\delta_{l'm'}\delta_{\nu\nu'},\\
B^{34}_{\mu\nu,\mu'\nu'}(ll';mm') &= \alpha^{*}_{l';\nu'\nu}\delta_{lm}\delta_{l'm'}\delta_{\mu\mu'},
\end{aligned} \tag{A8}$$

$$\begin{aligned}
B^{41}_{\mu\nu,\mu'\nu'}(ll';mm') &= 0,\\
B^{42}_{\mu\nu,\mu'\nu'}(ll';mm') &= -\alpha_{l;\mu'\mu}\delta_{lm}\delta_{l'm'}\delta_{\nu\nu'},\\
B^{43}_{\mu\nu,\mu'\nu'}(ll';mm') &= \alpha_{l';\nu\nu'}\delta_{lm}\delta_{l'm'}\delta_{\mu\mu'},\\
B^{44}_{\mu\nu,\mu'\nu'}(ll';mm') &= \widetilde{T}^{\nu\nu'\uparrow}_{l'm'}\delta_{lm}\delta_{\mu\mu'} - (\widetilde{T}^{\mu\mu'\downarrow}_{lm})^{*}\delta_{l'm'}\delta_{\nu\nu'}.
\end{aligned} \tag{A9}$$

---

[1] R. Arias and D. L. Mills, Phys. Rev. B **60**, 7395 (1999); A. Azevedo, A. B. Oliveira, F. M. de Aguiar, and S. M. Rezende, *ibid.* **62**, 5331 (2000); D. L. Mills and S. M. Rezende, *Spin Dynamics in Confined Magnetic Structures II* (Springer-Verlag, Heidelberg, 2002); P. Landeros, R. E. Arias, and D. L. Mills, Phys. Rev. B **77**, 214405 (2008); J. Lindner, I. Barsukov, C. Raeder, C. Hassel, O. Posth, R. Meckenstock, P. Landeros, and D. L. Mills, *ibid.* **80**, 224421 (2009).

[2] Y. Tserkovnyak, A. Brataas, and G. E. W. Bauer, Phys. Rev. Lett. **88**, 117601 (2002); Phys. Rev. B **66**, 224403 (2002); D. L. Mills, *ibid.* **68**, 014419 (2003); M. Zwierzycki, Y. Tserkovnyak, P. J. Kelly, A. Brataas, and G. E. W. Bauer, *ibid.* **71**, 064420 (2005)

[3] S. M. Rezende, A. Azevedo, M. A. Lucena, and F. M. de Aguiar, Phys. Rev. B **63**, 214418 (2001).

[4] R. Vollmer, M. Etzkorn, P. S. Anil Kumar, H. Ibach, and J. Kirschner, Phys. Rev. Lett. **91**, 147201 (2003); for a theoretical discussion of the linewidth and dispersion observed in the experiment, see A. T. Costa, R. B. Muniz, and D. L. Mills, Phys. Rev. B **70**, 054406 (2004).

[5] Early papers are H. Tang, M. Plihal, and D. L. Mills, J. Magn. Magn. Mater. **187**, 23 (1998); R. B. Muniz and D. L. Mills, Phys. Rev. B **66**, 174417 (2002); A. T. Costa, R. B. Muniz, and D. L. Mills, *ibid.* **68**, 224435 (2003).

[6] For an explicit comparison between the predictions of the Heisenberg model and that of an itinerant electron description of the spin excitations, see Figs. 4 and 5 of the theoretical paper cited in Ref. 4.

[7] S. Blügel, M. Weinert, and P. H. Dederichs, Phys. Rev. Lett. **60**, 1077 (1988).

[8] S. Heinze, M. Bode, A. Kubetzka, O. Pietzsch, X. Nie, S. Blügel, and R. Wiesendanger, Science **288**, 1805 (2000).

[9] M. Bode, M. Heide, K. von Bergmann, P. Ferriani, S. Heinze, G. Bihlmayer, A. Kubetzka, O. Pietzsch, S. Blügel, and R. Wiesendanger, Nature (London) **447**, 190 (2007).

[10] L. Udvardi and L. Szunyogh, Phys. Rev. Lett. **102**, 207204 (2009).

[11] Kh. Zakeri, Y. Zhang, J. Prokop, T. H. Chuang, N. Sakr, W. X. Tang, and J. Kirschner, Phys. Rev. Lett. **104**, 137203 (2010).

[12] P. Lederer and A. Blandin, Philos. Mag. **14**, 363 (1966).

[13] See also A. T. Costa, R. B. Muniz, and D. L. Mills, Phys. Rev. B **74**, 214403 (2006).

[14] A. T. Costa, R. B. Muniz, and D. L. Mills, Phys. Rev. B **73**, 054426 (2006).

[15] A. Bergman, A. Taroni, L. Bergqvist, J. Hellsvik, B. Hjörvarsson, and O. Eriksson, Phys. Rev. B **81**, 144416 (2010).

[16] E. Abate and M. Asdente, Phys. Rev. **140**, A1303 (1965).

[17] P. Fulde and A. Luther, Phys. Rev. **175**, 337 (1968).

[18] See the discussion in the second paper cited in footnote 5.

[19] See M. Tinkham, *Group Theory and Quantum Mechanics* (McGraw Hill, New York, 1964), Chaps. 6 and 7, Appendix C.

[20] See D. M. Edwards, in *Moment Formation in Solids*, NATO Advanced Study Institute, Series B: Physics Vol. 117, edited by W. J. L. Buyers (Plenum, New York, 1984), page 114.

[21] See the second and third papers cited in footnote 5.

[22] A. T. Costa, R. B. Muniz, J. X. Cao, R. Q. Wu, and D. L. Mills, Phys. Rev. B **78**, 054439 (2008).

[23] J. Prokop, W. X. Tang, Y. Zhang, I. Tudosa, T. R. F. Peixoto, Kh. Zakeri, and J. Kirschner, Phys. Rev. Lett. **102**, 177206 (2009).

[24] W. X. Tang, Y. Zhang, I. Tudosa, J. Prokop, M. Etzkorn, and J. Kirschner, Phys. Rev. Lett. **99**, 087202 (2007).

[25] See the discussion in A. T. Costa, R. B. Muniz, and D. L. Mills, IEEE Trans. Magn. **44**, 1974 (2008).

[26] S. Krause, G. Herzog, T. Stapelfeldt, L. Berbil-Bautista, M. Bode, E. Y. Vedmedenko, and R. Wiesendanger, Phys. Rev. Lett. **103**, 127202 (2009).

[27] M. Pratzer, H. J. Elmers, M. Bode, O. Pietzsch, A. Kubetzka, and R. Wiesendanger, Phys. Rev. Lett. **87**, 127201 (2001).

[28] N. Papanikolaou, R. Zeller, and P. H. Dederichs, J. Phys.: Condens. Matter **14**, 2799 (2002).

[29] S. H. Vosko, L. Wilk, and M. Nusair, Can. J. Phys. **58**, 1200 (1980).

[30] A. I. Liechtenstein, M. I. Katsnelson, V. P. Antropov, and V. A. Gubanov, J. Magn. Magn. Mater. **67**, 65 (1987).

[31] P. R. Peduto, S. Frota-Pessôa, and M. S. Methfessel, Phys. Rev. B **44**, 13283 (1991).

[32] S. Frota-Pessôa, Phys. Rev. B **46**, 14570 (1992).

[33] R. Haydock, in *Solid State Physics*, edited by H. Ehrenreich, F. Seitz, and D. Turnbull (Academic Press, New York, 1980), Vol. 35.

[34] O. K. Andersen, Phys. Rev. B **12**, 3060 (1975).

[35] O. K. Andersen, O. Jepsen, and D. Glötzel, in *Highlights of Condensed Matter Theory*, edited by F. Bassani, F. Fumi, and M. P. Tosi (North-Holland, Amsterdam, 1985).

[36] U. von Barth and L. A. Hedin, J. Phys. C **5**, 1629 (1972).

[37] O. Eriksson, B. Johansson, R. C. Albers, A. M. Boring, and M. S. S. Brooks, Phys. Rev. B **42**, 2707 (1990).

[38] N. Beer and D. Pettifor, *The Electronic Structure of Complex Systems* (Plenum Press, New York, 1984).

[39] M. Plihal and D. L. Mills, Phys. Rev. B **58**, 14407 (1998).

[40] O. K. Andersen and O. Jepsen, Phys. Rev. Lett. **53**, 2571 (1984).

[41] M. Heide, G. Bihlmayer, and S. Blügel, Phys. Rev. B **78**, 140403(R) (2008).

[42] B. M. Hall and D. L. Mills, Phys. Rev. B **34**, 8318 (1986); B. M. Hall, D. L. Mills, M. H. Mohamed, and L. L. Kesmodel, *ibid.* **38**, 5856 (1988).

[43] M. P. Gokhale, A. Ormeci, and D. L. Mills, Phys. Rev. B **46**, 8978 (1992).

[44] B. M. Hall, S. Y. Tong, and D. L. Mills, Phys. Rev. Lett. **50**, 1277 (1983).

[45] R. Urban, G. Woltersdorf, and B. Heinrich, Phys. Rev. Lett. **87**, 217204 (2001).